



PCCP

Electronic properties of bare and functionalized Two-Dimensional Tellurene structures

Journal:	<i>Physical Chemistry Chemical Physics</i>
Manuscript ID	CP-ART-01-2020-000357.R1
Article Type:	Paper
Date Submitted by the Author:	04-Mar-2020
Complete List of Authors:	Wines, Daniel; University of Maryland Baltimore County, Physics Kropp, Jaron; University of Maryland Baltimore County, Physics Chaney, Gracie; University of Maryland Baltimore County, Physics Ersan, Fatih; Adnan Menderes University, Physics; University of Maryland Baltimore County, Physics Ataca, Can; University of Maryland Baltimore County College of Natural and Mathematical Sciences, Department of Physics

SCHOLARONE™
Manuscripts

Cite this: DOI: 00.0000/xxxxxxxxxx

Electronic properties of bare and functionalized Two-Dimensional Tellurene structures

Daniel Wines,^a Jaron A. Kropp,^a Gracie Chaney,^a Fatih Ersan,^{ab} and Can Ataca^{*a}

Received Date

Accepted Date

DOI: 00.0000/xxxxxxxxxx

Recently, 2D Tellurene (Te) structures have been experimentally synthesized. These structures possess high carrier mobility and stability which make them ideal candidates for applications in electronics, optoelectronics and energy devices. We performed density functional theory (DFT) and molecular dynamics (MD) simulations to investigate the stability and electronic structure of 2D α - and β -Te sheets, and hydrogen, oxygen, and fluorine functionalized counterparts, including spin-orbit coupling effects. Our calculations show that bare α and β -Te sheets are stable with band gaps of 0.44 eV and 1.02 eV respectively. When functionalized, α and β monolayers exhibit metallic properties, except for hydrogenated β -Te, which exhibits semiconducting properties with a band gap of 1.37 eV. We see that H, O and F destabilize the structure of α -Te. We also find that F and H cause β -Te layers to separate into functionalized atomic chains and O causes β -Te to transform into a Te_3O_2 -like structure. We also studied single atom and molecule binding on the Te surface, the effects of adatom coverage, and the effects of functionalized Te on a GaSe substrate. Our results indicate that Tellurene monolayers and functionalized counterparts are not only suitable for future optoelectronic devices, but can be used as metallic contacts in nanoscale junctions.

1 Introduction

In recent years, two-dimensional (2D) materials have been extensively studied due to their advantageous electronic properties which differ from their bulk form and their range of potential applications in electronic, optoelectronic and nanoscale junction applications^{1–3}. From the wide range of 2D materials, 2D mono-elemental materials such as group-IV and group-VA monolayers have attracted a particular interest due to their unique chemical and physical properties^{4–6}. Among these 2D mono-elemental materials exists group-VI Tellurene (Te), which has recently been investigated theoretically and experimentally synthesized^{7–10}. High carrier mobility and significant air stability make Tellurene a promising candidate for next generation devices^{7,10}.

Theoretical studies have shown that 2D Tellurene can exist in the α -Te phase (1T-MoS₂ like) and the tetragonal β -Te phase⁷. It has also been shown that when the thickness decreases to $N = 8$ (where N is the number of Tellurene layers), the geometric structure of bulk Te (γ -Te) transforms into multilayered α -Te after structural optimization. In contrast to α -Te, which is obtained from a thickness-dependent phase transition from bulk Te, β -Te occurs as a natural result of structural relaxation when

the bulk Te structure is truncated along the [100] or [010] directions into thin films at the correct thickness⁷. The α -Te and β -Te phases possess a nearly-direct and direct band gap, respectively, which results in enhanced optical absorption properties. Both of these phases also possess higher hole carrier mobilities ($1.76 \times 10^3 \text{ cm}^2 \text{ v}^{-1} \text{ s}^{-1}$ for α -Te and $1.98 \times 10^3 \text{ cm}^2 \text{ v}^{-1} \text{ s}^{-1}$ for β -Te) than 2H-MoS₂, which has a hole carrier mobility of $0.29 \times 10^3 \text{ cm}^2 \text{ v}^{-1} \text{ s}^{-1}$. Theoretical studies have indicated that certain structures such as square Tellurene exhibit topological insulating properties, hosting non-trivial edge states¹¹ and experimental studies have confirmed that 2D α -Te exhibits topological insulating properties¹². First-principles calculations also indicate that 2D Tellurene is an excellent thermoelectric material with a high room temperature Seebeck coefficient ($S_{xx} = 0.38 \text{ mV/K}$, $S_{yy} = 0.36 \text{ mV/K}$), and an anisotropic lattice thermal conductivity ($\kappa_{xx}^1 = 0.43 \text{ W/mK}$, $\kappa_{yy}^1 = 1.29 \text{ W/mK}$)¹³. Additionally, the Quantum Hall effect can be observed in few layer 2D Tellurene ($\sim 10 \text{ \AA}$ thick flakes) under high magnetic field ($\sim 5\text{--}20 \text{ T}$)¹⁴.

Quasi-2D structures such as high-mobility Te nanoflakes have been solution-synthesized with potential applications for short-wave infrared photodetectors (SWIR). Although these nanoflakes possess an indirect band gap, they can be utilized for SWIR photodetectors when placed on optical cavity substrates (such as Au/Al₂O₃) to increase the absorption in the semiconductor¹⁵. First-principles calculations have determined that by applying strain, phase transitions and mechanical property modulations

^aDepartment of Physics, University of Maryland Baltimore County, Baltimore MD 21250; E-mail: ataca@umbc.edu

^bDepartment of Physics, Aydin Adnan Menderes University, Aydin 09100, Turkey.

† Electronic Supplementary Information (ESI) available: [details of any supplementary information available should be included here].

can be induced in 2D Tellurene^{16,17}. Recently, the effects of adatoms and gas molecules such as H₂, O₂, NO₂, H₂O, and NH₃ on the surface of α -Te and β -Te monolayers at dilute doping concentrations have been theoretically studied and the effects on the electronic structure have been reported¹⁸. The results of this study indicate that while most adatoms are chemisorbed on Te sheets with large adsorption energies, some adatoms such as Ca, Fe, Co, and Ni give rise to structural deformations and local reconstructions which result in different induced electronic structures. These calculations also show that all considered gas molecules are physisorbed on Te sheets and have a weak effect on the electronic structure¹⁸.

Previous studies have also indicated that functionalization by dense doping of impurities can tune the electronic properties of certain 2D materials^{19–24}. For example, σ -character Dirac cones can be engineered in phosphorene (2D phosphorous) when the material is single- and double-side hydrogenated and fluorinated²¹. Similarly when 2D monolayer arsenic (arsenene) is hydrogenated, the same σ -type Dirac cones have been predicted²². Theoretical studies also indicate that the oxidation of 2D antimony (antimonene, an indirect semiconductor), can tune the band gap to direct and widen the band gap value depending on the concentration of oxygen added¹⁹. Interesting electronic properties arise when group-III monochalcogenides, which possess wide band gaps in the visible region (2.04 eV - 3.47 eV), are functionalized with oxygen atoms. After oxygen functionalization, the band gaps of these group-III monochalcogenides decrease (under 1 eV). Double-site oxygen functionalization causes InS, InSe and InTe to become 2D topological insulators with sizable band gaps (up to 0.21 eV)²⁵.

In this study, motivated by how hydrogenation, oxidation and fluorination modify the properties of certain other 2D materials^{19–24}, we investigated the stability, structural and electronic properties of 2D bare and functionalized Tellurene structures using density-functional theory (DFT) and *ab-initio* molecular dynamics (MD) calculations within the projector augmented-wave method^{26,27}. For bare 2D α -Te and β -Te sheets, we calculated band gaps of 0.44 eV and 1.02 eV, respectively. When functionalized with H, O, and F atoms, the band gaps of 2D α -Te and β -Te decrease and the structures become metallic except hydrogenated β -Te, which remains semiconducting, but now has a band gap of 1.37 eV. From our phonon dispersion and MD simulations, we found that oxygenated β -Te is stable and hydrogenated β -Te is meta-stable. We also report that H, O, and F functionalization fully disrupts the structure of α -Te. Additionally, H and F functionalization causes the β -Te layers to separate into functionalized chains, and O causes a total structural transformation of β -Te to a Te₃O₂-like structure. To investigate these structural changes further, we calculated the binding/dissociation energies of single H, O and F atoms and single H₂, O₂, and F₂ molecules on monolayer α and β -Te. To gain an understanding of how adatom coverage effects the stable Te structures, we varied the H and O coverage of bare β -Te and found that fully functionalized O- β -Te and H- β -Te have the strongest adatom binding energies. We also performed MD simulations for high coverage of H₂, O₂, and F₂ (six-eight molecules on each side) on the α and β -Te surfaces. To

extend our simulations to more realistic systems, we studied the effects of the stable functionalized Te structures (O- β -Te and H- β -Te) on a GaSe substrate. We found that the stability of layered Te structures are enhanced since these structures bind strongly to GaSe surface and remain intact. Our results confirm that 2D Tellurene structures are excellent candidates for metallic contacts in nanoscale junctions and are suitable for next generation optoelectronic devices.

2 Computational Details

Our theoretical calculations were obtained via first-principles pseudopotential calculations based on spin-polarized density-functional theory within the generalized gradient approximation (GGA), and including van der Waals (vdW) corrections using the DFT-D2 method²⁸ and spin-orbit coupling (SOC) effects. We used projector augmented-wave (PAW) potentials and approximated the exchange-correlation potential with the Perdew-Burke-Ernzerhof (PBE) functional^{27,29}. The Vienna *ab initio* simulation package (VASP) code was used for numerical calculations²⁶. The kinetic energy cutoff of our plane-wave basis set was taken to be $\hbar^2 |\mathbf{k} + \mathbf{G}|^2 / 2m = 450$ eV. The Monkhorst-Pack scheme was used to sample the Brillouin zone (BZ) using a 20×20×1 mesh in \mathbf{k} space for 2D structures³⁰. The number of \mathbf{k} -points was scaled accordingly with the size of the supercell in our simulations. Atomic positions were optimized using the conjugate gradient method, where the total energy and the atomic forces were minimized. A maximum force of 0.01 eV/Å was allowed on each atom and the energy convergence value between two consecutive steps was chosen to be 10⁻⁵ eV. The vacuum spacing between periodic layers was set to at least 20 Å to minimize inter-layer coupling. The Gaussian-type Fermi-level smearing method is used with a smearing width of 0.01 eV. Self-consistent field calculations of the electronic band structure and the total and orbital projected density of states (with the smearing width increased to 0.05 eV) were carried out including SOC effects. The cohesive energy of each structure is obtained by the expression $E_{coh} = (nE_{Te} + mE_{atom} - E_{2D-Te}) / (n + m)$, where E_{Te} , E_{atom} and E_{2D-Te} are the isolated total energy of the free Te atoms, the isolated total energy of the functionalization atoms (H, O, F) and the total energy of the bare/functionalized 2D Te structures respectively. The number of Te atoms and adatoms in the cell are labeled as n and m , respectively. The phonon dispersion curves were obtained using the finite-displacement method (4×4×1 supercell for α -Te, 4×3×1 for β -Te) implemented in the PHONOPY code³¹. In phonon dispersion simulations, SOC effects are excluded due to computational limitations. For single atom and molecule adsorption simulations we used a 4×4×1 supercell for α -Te and a 4×3×1 supercell for β -Te. The thermal stability of our optimized structures was also tested using finite-temperature *ab initio* molecular dynamics simulations at 300 K and 600 K with a time step of 0.5 fs. These simulations were run at time scales of 3 - 8 ps and used the Nosé-Hoover thermostat to obtain the canonical (NVT) ensemble. Bader charge analysis was used to obtain the charge distribution on the atoms in our simulations^{32,33}. The VESTA program was used to visualize of the atomic structures³⁴. To calculate electronic transport coefficients such as the Seebeck

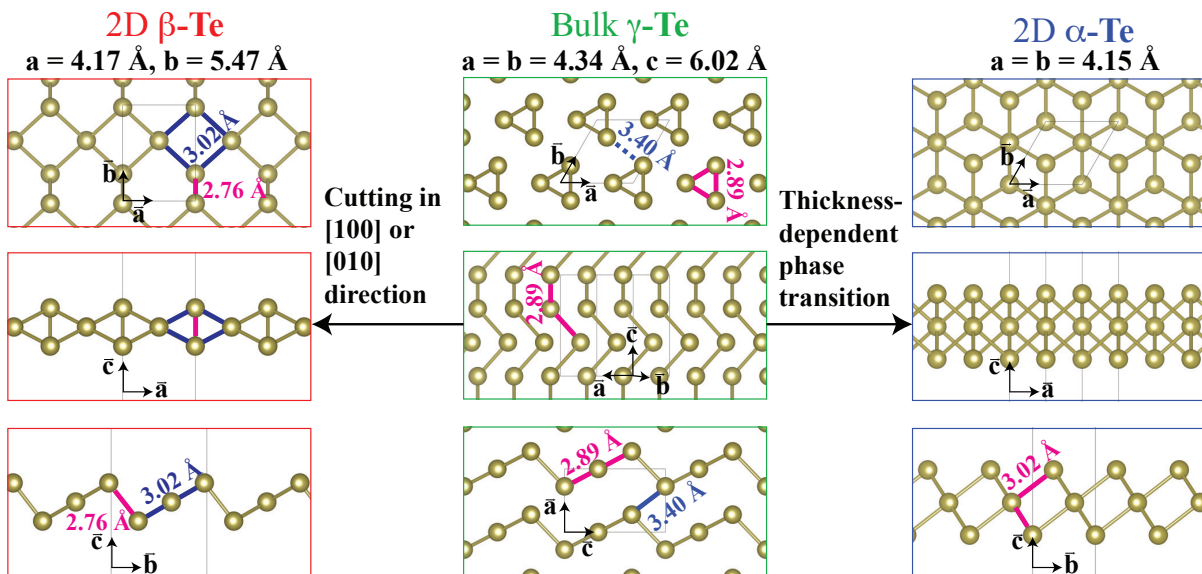


Fig. 1 Top and side views of the helical chain structure of of bulk γ -Te (middle column), the rectangular structure of monolayer β -Te (left column), and the hexagonal structure of monolayer α -Te (right column), respectively. Bond lengths (represented by pink and blue lines), lattice parameters and interchain distances are given in the insets.

coefficient (S), we used semiclassical Boltzmann transport theory (BTT) within the constant relaxation time approximation and the rigid band approach as implemented in the BoltzTraP2 code.^{35,36}

3 Results and Discussion

3.1 Bare 2D Te

Bulk Tellurium (γ -Te) has a space group of $P3_121$. The unit cell of γ -Te contains three two-fold coordinated Te atoms that form helical chains parallel to the c -axis with a bond distance of $d_{Te-Te} = 2.89$ Å. The calculated lattice parameters of γ -Te are $a = b = 4.34$ Å, $c = 6.02$ Å and the structure is depicted in Fig. 1. As the number of Te layers decreases in the γ -Te, the helical chains become closer together and the structure turns to α -Te with a space group of $P\bar{3}m1$. The decreased distance between helical chains results in a bond distance of $d_{Te-Te} = 3.02$ Å with lattice parameters of $a = b = 4.15$ Å. Another stable form of Tellurium known as β -Te (Fig. 1) has space group $P2/m$. This structure arises from the cutting of Te-Te bonds in bulk γ -Te along the $[100]$ or $[010]$ direction. This results in two bond distances of $d_{Te-Te} = 2.76$ Å and $d_{Te-Te} = 3.02$ Å with lattice parameters of $a = 4.17$ Å and $b = 5.47$ Å. The van der Waals (vdW) radius of Tellurium is 2.06 Å³⁷ and the average bond distance of our present structures is ~ 2.9 Å. A purely van der Waals interaction would have bond lengths of ~ 4.1 Å, so this implies there is stronger bonding between Te atoms including metal-ligand multiple and covalent bonds.

Monolayer β -Te has both three-fold and four-fold bonds and α -Te has three-fold and six-fold bonds, whereas bulk γ -Te has two-fold bonds (inside chains). Increasing from two-fold bonds to higher bond order results in a decrease in cohesive energy of the Te structures and bond strength and an increase in bond length. For instance, calculated cohesive energy with (without) SOC of γ -

Te is 2.35 (2.80) eV/atom, while this value is 2.26 (2.63) and 2.23 (2.58) eV/atom for 2D α -Te and β -Te (on average) monolayers, respectively. In order to relate bond energy to the number of fold bonds, we calculated bond breaking energy for all 2D-Te structures with SOC. For γ -Te in which all the bonding in the chain-like structure is the same and covalent in character and weak interaction between chains, bond energy is calculated as 0.97 eV/bond (calculated by $(d * E_{coh} - E_b)/(n * d)$ where n the number of folding of bonds, d is the number of Te atoms in the primitive cell and E_b is the interchain binding energy which will be discussed in the upcoming subsection). For α - and β -Te, we calculate the bond energy of the n -fold bonds as $E_{BE} = (E_{vac} + E_{Te_{coh}} - E_{2D})/n$, where E_{2D} is the energy of the pristine 2D layer, E_{vac} is the energy of the vacancy-containing layer, and $E_{Te_{coh}}$ is the cohesive energy of a Te atom obtained from γ -Te. For α -Te, there exists a metal-ligand-like bonding between the central atom (six-fold) and the outer atoms (three-fold). The bond energy of the three-fold and six-fold bonded Te atoms in α -Te are 0.75 eV/bond and 0.62 eV/bond, respectively. For the β -Te monolayer, the outer atoms have three-fold bonding: two with a metal-ligand-like bonding with two neighboring central atoms and one with a strong σ bonding between upper and lower atoms. The central atoms have four metal-ligand-like bonding to the neighboring outer atoms. The average bond energy of the three-fold and four-fold bonded Te atoms in β -Te are 0.77 eV and 0.66 eV, respectively. From these calculations, we conclude that Te atoms prefer to bond with lower bond order which results in lower bond length and higher cohesive energy per bond.

For the sake of comparison with the literature, we also calculated the electronic band structures of bare Te structures. Our calculations indicate that γ -Te has an indirect band gap of 0.31 eV, while β -Te has an indirect band gap of 1.17 eV and α -Te has

an indirect band gap of 0.76 eV. Similar to other mono-elemental materials from the fifth row of the periodic table such as Sb³⁸, SOC becomes dominant in the electronic band structures of Te materials because of an increase of *d*-orbitals in Te atoms⁷. As a result, SOC decreases these band gap values by 0.15 eV for β -Te and 0.32 eV for α -Te and turns them to direct gap semiconductors as shown in Supplementary Information (SI) Fig. S1. These values are comparable with previous theoretical results⁷. Because of these significant changes to the electronic structure when SOC is taken into account and due to the heavy atomic mass (atomic number) nature of Te atoms⁷, we carried out all numerical calculations (except phonon dispersion curves due to computational limitations) including SOC effects. A full description of the underlying physics of SOC in Te-based materials can be found in the following references^{7,11,39–41}.

In addition to SOC, we also employed vdW corrections to the energy in all of our simulations. Although it is a common misconception that vdW corrections are only needed in multi layer/bulk systems, monolayer materials require this correction to correctly describe the long-range interactions. This is especially needed in 2D Te structures, where functionalization causes the structure to either separate into chains or layers (this will be discussed in detail in the next subsection). This separation results in a weak vdW interaction between the chains/layers that requires a correction to the energy.

3.2 Functionalized 2D Te Structures

3.2.1 Modification of atomic structure upon functionalization

Functionalized 2D Tellurene structures may exhibit different properties than their bare 3D bulk and 2D counterparts. Therefore, to investigate the effects of the functionalization of α - and β -Te monolayers at high adatom concentrations, we placed H, O, or F atoms 2 Å above each outer Te atom in the primitive cell and performed geometric optimization calculations. Figure 2 shows the cohesive energies of H and O functionalized β -Te structures as a function of lattice constant (for the *a* direction) while Fig. S2 depicts all of the considered H, O, and F α - and β -Te structures as a function of lattice constant. As seen in Fig. 2 and Fig. S2, all functionalized structures except O- β -Te have a local minimum and a global minimum at different lattice constant values. All global minima structures indicate that functionalization results in a decrease of the lattice constant.

For all the functionalized α structures, the bare α -Te shape is preserved at the local minimum while the Te layers separate at the global minimum with an average *c* distance of 3.29 Å between each layer (as compared to an interlayer distance of \sim 1.8 Å for bare 2D α -Te). The compression of the lattice constants along the *a* and *b*-axes lead to stronger nearest-neighbor interactions between Te atoms in the same plane. This change in bonding environment leads to a separation of the layers along the *c*-axis (out of plane movement of the surface Te atoms), which results in a new charge distribution in the structure. Bader analysis indicates that, for the H- α -Te at the local minimum, both H atoms accept 0.23 electrons (e^-) from the Te atoms. The outer (surface) Te

atoms donate 0.19 e^- each and the inner Te atom donates 0.09 e^- . However, for the H- α -Te at the global minimum, the inner Te atom takes 0.20 e^- from the outer Te atoms. Therefore the inner Te layer becomes negatively charged and this charge transfer results in polarization between Te layers. The calculated charge transfer values are higher for O and F functionalization. Each O atom takes 0.80 e^- and each F atom takes 0.61 e^- from the outer layer of Te atoms at the respective local minimum. These values are slightly lower for the global minimum of each structure because the inner Te atoms also accept electrons from the outer Te atoms. The effects of lattice compression and modification of charge transfer between Te layers on the electronic structure of Te monolayers will be discussed in the further subsections.

The functionalization of β -Te structures results in different structural changes when compared to that of α -Te. For H- β -Te, functionalization causes the strong covalent bond between outer Te atoms to break (as highlighted by orange dashed lines in the Fig. 2 and S2 insets) at both minima. This causes the structure to change drastically at the global minimum to one composed of parallel, planar H-Te chains extending along the *a*-axis. These chains are highlighted with green ellipses in Fig. 2 and Fig. S2. However, we note that there is a negligible difference in cohesive energy between the local and global minima of H- β -Te of only 4 meV/atom. We attribute this to both structures at each minimum having a H-Te chain structure with only slightly different chain-chain distances (both are larger than twice of Te atoms vdW radius) and angles between the *c*-axis and *a*-*b* plane. F- β -Te exhibits a similar structural transition as H- β -Te. Since the functionalized chains are weakly bonded, the Bader charge analysis report similar charge distribution in both chain structures. H and F atoms get charges from outer Te atoms and negatively charged by \sim 0.17 and \sim 0.62 electrons, respectively.

To further analyze the chain-like nature of the H- and F- β -Te structures, we calculated the interchain binding energies and compared the values to that of γ -Te, which is proposed to be formed of covalently bonded chains⁴². The interchain binding energy is defined as $E_b = E_{chain} - E_{Te}$ where E_{chain} is the total energy of the isolated functionalized H- or F-Te chain and E_{Te} is the total energy of the functionalized 2D β -Te structures (at the local or global minima). The calculated E_b for the bulk chain structure (γ -Te) is 1.26 eV, which is in good agreement with the literature⁴². In contrast, we find values for H-Te of $E_b=0.24$ eV at the local minimum and 0.27 eV at the global minimum. For F-Te, $E_b=0.31$ eV at the local minimum and 0.32 eV at the global minimum. These values are lower than that of γ -Te and thus indicate weak chain-to-chain interaction in hydrogenated and fluorinated β -Te. They also support our discussion why local and global minimum structures are energetically very close and the chains are bonded dominantly by vdW interaction.

Oxidation of Te results in a different structural transformation for β -Te. For O- β -Te, the O atoms break the Te-Te bond, penetrate into the Te layers, and bond to the outer two Te atoms, resulting in a Te₃O₂-like structure. This structural transformation results in a buckling of Te atoms on the *c* axis with a singular global minimum. The highest amount of charge transfer (1.07 e^- from Te atoms to the O atoms) occurs with this structural transformation.

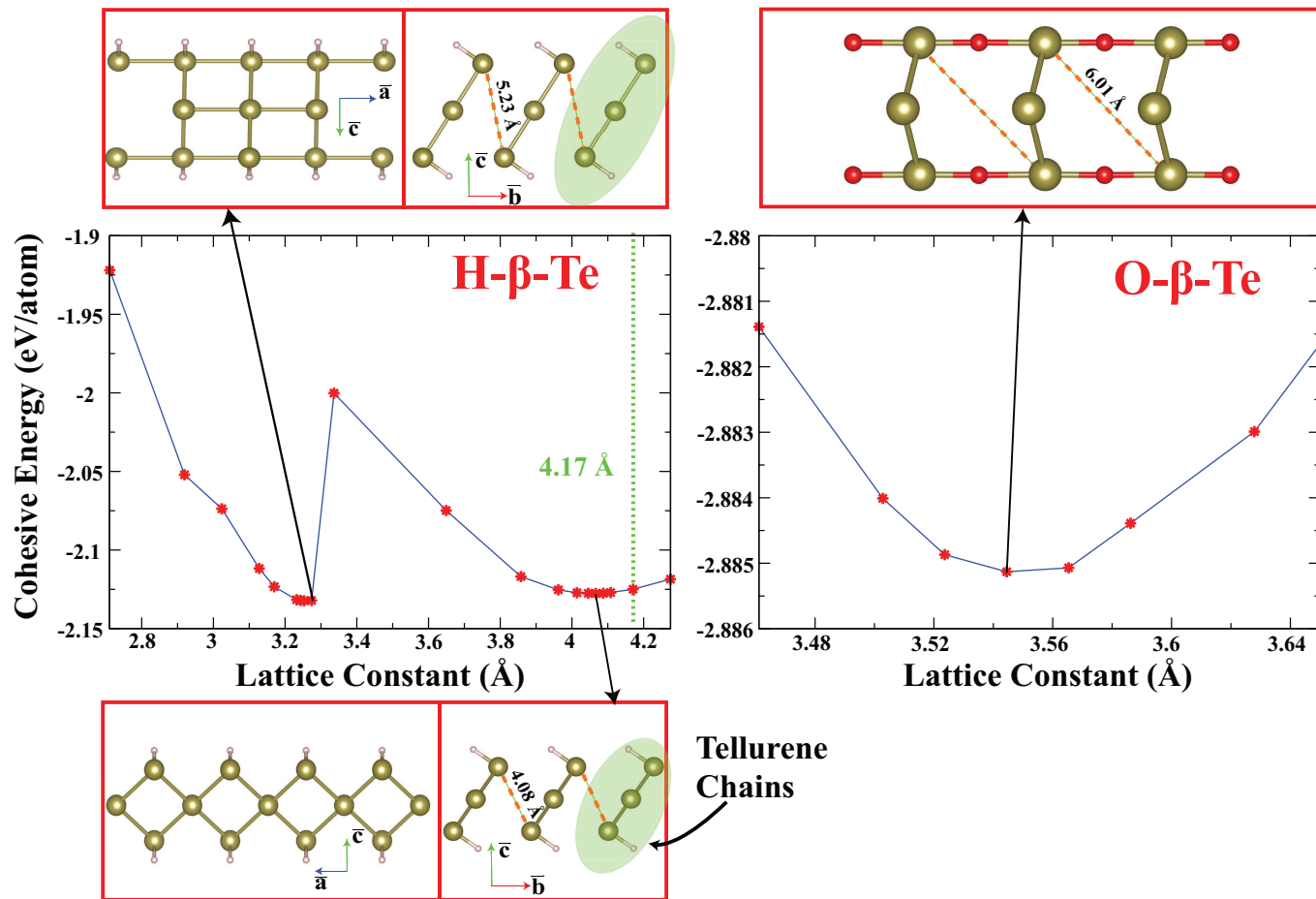


Fig. 2 The cohesive energy (in eV/atom) as a function of lattice constant (for the \bar{a} direction) for 2D β -Te functionalized with H and O. We observe one local and one global cohesive energy minimum for H- β -Te and a single global minimum for O- β -Te. The optimized geometry of the functionalized Tellurene structures at each minimum are depicted above and below the corresponding energy landscape. Bond breaking is indicated by the orange dashed lines. The green dashed lines on cohesive energy plots represent the lattice constant (in the \bar{a} direction) for bare monolayer β -Te (bottom row).

For this new structure, inner site Te atoms also lose $0.12 e^-$ and donate to O atoms.

3.2.2 Stability analysis

It has previously been stated that two methods to filter out stable 2D materials include the calculation of the phonon dispersion relation for the whole BZ and ensuring there are no negative frequencies and performing an *ab-initio* Molecular Dynamics simulation to test dynamical stability at finite temperatures⁴³. Applying just one of these filters cannot guarantee stability, but using both in conjunction with one another can provide strong insight to whether or not a 2D structure is stable.

To investigate the stability of the functionalized α and β structures at each minimum, we first performed phonon calculations. Obtained phonon dispersion curves indicate that O- β -Te has positive phonon frequencies for the whole BZ (Fig. 3b). For H- β -Te, we observe that the global minimum contains a larger number of negative frequencies than the local minimum [Fig. S3b (global minimum) vs Fig. 3a (local minimum)]. The atomic movements and the phonon partial density of states (PDOS) indicate that the instability is not related with the Te-H bonds, but due to the

breaking of strong covalent bonding between outer Te atoms. The lack of restoring force for the rotation of Te_3H_2 chains causes the instability. Similar instability is also observed for the global minimum H- β -Te structure. This slight instability can easily disappear if the H- β -Te structure is placed on a suitable substrate such as graphene, Cu, Ni, Pt, GaS, or GaSe^{8,44,45}. Recently, Yang et al.⁴⁵ showed that bare Te sheets can be synthesized on GaSe substrates and that they are well-oriented along the GaSe armchair lattice direction⁴⁵. Theoretically and experimentally, it has also been proposed that Tellurene monolayers can be stabilized by CdTe interfaces⁴⁶. We will also discuss the stabilization of functionalized Te monolayer by substrates in further subsections. The remaining phonon dispersion curves indicate that F- β -Te and all functionalized α structures are unstable due to the presence of a larger number of negative phonon frequencies (Fig. S3).

We investigated the atomic movements of our functionalized structures at the special high symmetry points to elucidate the exact nature of the observed instabilities in the other functionalized Tellurene structures. The H- α -Te structure at its local minimum (Fig. S3a) exhibits four negative frequency bands for the

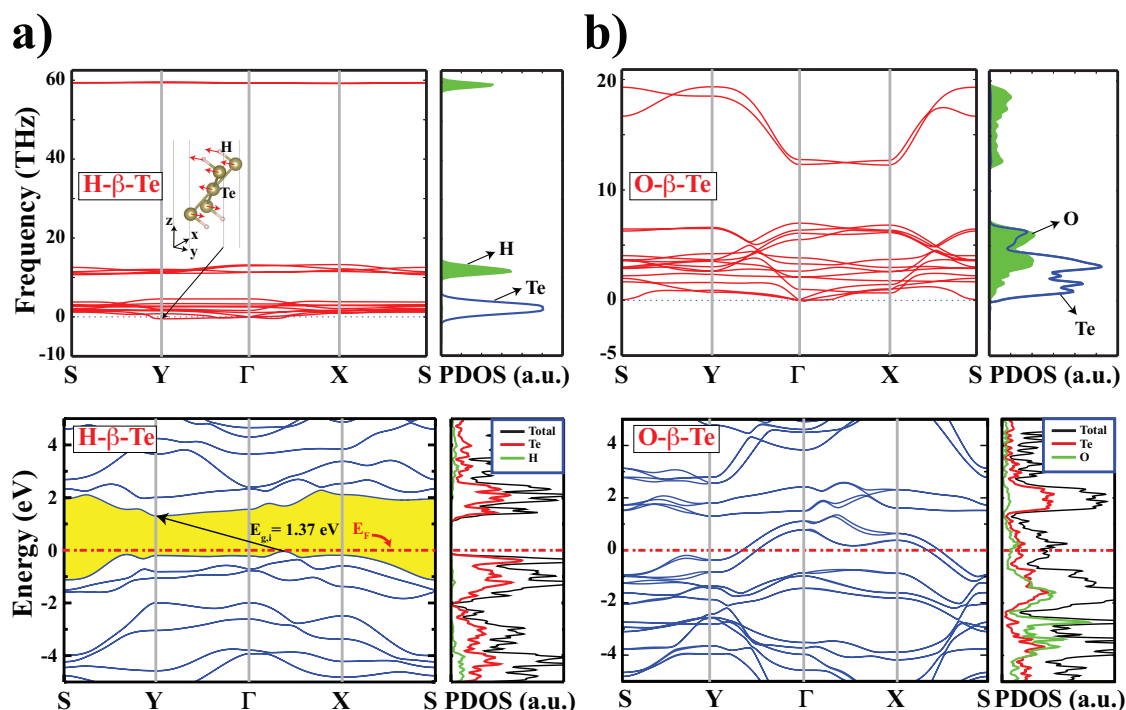


Fig. 3 The phonon band structure and phonon projected density of states (PDOS), in addition to the electronic band structure and orbital projected density of states (PDOS) of a) H- β -Te at its local energy minimum and b) O- β -Te at its singular global energy minimum. For H- β -Te, the atomic movements at the negative frequency at the Y high symmetry point are shown (red arrows depict the vibration direction).

whole BZ. At the M point, the lowest two frequencies correspond to out of phase movements of the H atoms about stationary Te atoms. Since there is no restoring force keeping these H atoms from moving back to equilibrium, the structure will break apart. The remaining two modes are from the Te atoms moving out of phase. At its global minimum, H- α -Te has three negative acoustic modes for the whole BZ originating only from Te atoms. This implies that the H- α -Te structure at the global minimum wants to change its structural shape due to high compressive strain.

As discussed in the previous section, O and F adatoms withdraw significant electrons from the α -Te structure and at global minimum structures, they result in separation of Te layers. For the local minimum of O- α -Te, whole BZ features three negative acoustic phonon bands. For the negative frequency with the largest value at the M point, one Te atom on the bottom of the structure moves in the opposite in-planar direction from the other Te atoms. The global minimum for O- α -Te has three negative acoustic modes which consists of out of plane atomic movements due to increase in the interlayer distances. F adatoms destroy all layered Te structures. Unlike O, instability of structures are also originating from F adatoms. In regards to F- α -Te, both the local and global minima have five negative frequency bands that are a mixture of acoustic and optical modes. The global and local minima for F- β -Te feature negative acoustic modes spanning the whole BZ. In addition to weakening of the covalent bonding between Te atoms on the outer edges like H- β -Te, F adatoms are destabilizing the structure by out-of-phase vibrations (see Fig. S3).

To further examine the stability of the structures which con-

tained negative phonon frequencies, we performed *ab-initio* Molecular Dynamics simulations at a finite temperature of 300 K and a time scale of 3 ps with a time step of 0.5 fs. After 3 ps, we observed significant disruption of the structures, which confirm our stability calculations. For O- β -Te, we observe no disruption to the structure with the O atoms oscillating in the c-direction. For H- β -Te at the local minimum we observe no disruption until 2 ps and minimal disruption after 3 ps, with some H dissociating from the surface. This might signify that at lower H atom doping concentrations on Te monolayers, functionalized structures can be stable. We will discuss the effects of surface coverage in the upcoming subsections. Since O- β -Te and the local minimum of H- β -Te both satisfy the phonon and dynamical stability tests (aside from the small negative frequency of H- β -Te that can be lifted by a substrate), we can say with confidence that these two structures are stable and therefore we will study them in more detail in subsequent sections.

3.2.3 Electronic Properties of Functionalized 2D Te

For all the structures considered, we calculated the electronic band structures and partial density of states (PDOS) with spin-orbit coupling effects. The band structures and corresponding PDOS of the structures that contain negative frequencies in the phonon dispersion curves (unstable structures) are located in Fig. S4.

Although the cohesive energy difference between the local and global minima of H- β -Te is very small, the structural differences between these two minima have a significant effect on the electronic band structure. At the local minimum we observe an indi-

rect band gap of 1.37 eV (Fig. 3a), while at the global minimum H- β -Te has metallic characteristics (see Fig. S4). The metallic channel in the global minimum originates from the shortened middle layer Te bonds which provides further evidence for the dual character of Te bonds⁷. At the local minimum we see the valence band maximum (VBM) shift away from the Γ point and toward the X point (when compared with the band structure of bare β -Te). However, the conduction band minimum (CBM) remains at the same high symmetry point (Y). From the PDOS we see that the 1s H orbitals are mainly located below -4 eV. The VBM is dominated by p_x and p_y orbitals of Te atoms while the CBM is dominated by p_x and p_z orbitals of Te. The difference in the electronic structure between bare β -Te and H- β -Te at local minimum arises from the absence of strong covalent bonding between lower and upper Te layers. Fig. S5a) depicts the charge difference of H- β -Te (local min.) where yellow isosurfaces correspond to charge accumulation and blue isosurfaces correspond to charge depletion. We see that electrons are transferred from outer Te atoms to H atoms while there is a small amount of electron accumulation around the central Te atoms. The total charge density for H- β -Te (local min.) is also depicted (black contours correspond to the [100] plane at the origin while red contours correspond to the [100] plane cutting through the halfway point of the unit cell). Black contour lines show the weakened bonding between upper and lower Te atoms and formation of a strong bond between outer Te and H atoms. The band gap in the near infrared region makes H- β -Te ideal for optoelectronic devices and applications.

In Fig. 3b) we see that fully oxygenated Te has a metallic character and oxygen p states give a similar contribution as Te p states. The amount of charge transferred from Te to O is much larger than the charge transferred from Te to H in H- β -Te (local min.) and we have significant charge accumulation around the embedded O atoms and a significant charge depletion around the outer Te atoms (as seen in Fig. S5b)). This considerable transfer of electrons from outer Te atoms to O provides a viable explanation to why O functionalization causes such a significant structural transformation to a Te₃O₂-like structure. Even though the metal-ligand-like bonding between the middle and outer Te atoms are preserved, outer Te and O atoms have ionic bond character instead of the strong covalent bonding between upper-lower Te layers. This ionic bonding between Te and O results in states around the Fermi level. Because O- β -Te is a stable form of metallic 2D Tellurene, it is suitable for metallic contact applications in nanoscale junctions.

The additional O- α -Te band structures and PDOS at the local and global minima in Fig. S4 are also metallic, which proves that oxygen functionalization causes all Te structures to become metallic. We also calculated the Seebeck coefficient of the most stable functionalized structures (H- β -Te local min. and O- β -Te) and bare β -Te (for comparison) at 300 K using the BoltzTraP2 code in conjunction with PBE results. Previously, the thermoelectric properties of bare β -Te have been studied by Sharma et al.¹³ where BoltzTraP was used in conjunction with hybrid functional results to obtain a value of $S_{xx} = 0.38, S_{yy} = 0.36$ mV/K. The differences from our results can be accounted for by the difference

in methodology and we can still observe meaningful trends from our PBE interpolated results when comparing bare and functionalized β -Te. For bare β -Te, we obtain a high Seebeck coefficient of $S_{xx} = S_{yy} = 1.27$ mV/K. H functionalization has little effect on the Seebeck coefficient ($S_{xx} = S_{yy} = 1.29$ mV/K for H- β -Te at the local minimum) while O functionalization causes the Seebeck coefficient to significantly decrease to $S_{xx} = S_{yy} = 0.07$ mV/K for O- β -Te due to structure change.

In addition to these structures, H- β -Te and F- β -Te structures with a similar atomic configuration to optimized O- β -Te were created by initially tilting the H or F atoms. The atomic structures after ab-initio geometry optimization are given in Fig. S6. Focusing initially on H- β -Te, we see that H atoms align planar with outer Te atoms of β -Te, however H atoms are not centered between neighboring Te atoms, being way more closer to one Te than the other (1.69 Å vs 2.71 Å). Examining this atomic structure in detail, we concluded that this structure is almost identical to local minimum H- β -Te. The minor differences arising from H atoms are tilted more and there is a slight lattice constant increase from ~ 4.10 Å to ~ 4.20 Å. This minor difference in geometric structure does not have a significant effect on the stability (phonon dispersion curves) and the electronic structure when Fig. 3a) and Fig. S6a) are compared.

For the case of F adatoms in O- β -Te like structure (see Fig. 3), the difference of the lattice structure and its effects on stability and electronic properties is significant. This new configuration of F- β -Te, indicated in Fig. S6b), has a fewer number of negative phonon frequencies when compared to the initial configuration in Fig. S3. For the F- β -Te structure, the top of the valence band (A, See Fig S6b) and the bottom of the conduction band (B, See Fig S6b) are 200 meV above and 130 meV below the Fermi level from PBE calculations. However, these values decreased to 77 meV for the B point and 83 meV for the A point after adding SOC effects to the calculations. This overlapping is a characteristic of semimetallic materials. Bader analysis indicates that each F atoms take 0.81 e⁻ from Te atoms and from these amounts of electrons, 0.10 e⁻ comes from the inner Te atom, and 0.71 e⁻ comes from outer Te atom.

3.3 Single atom and molecule binding and coverage effects

After phonon calculations revealed the stability of functionalized Te structures, we calculated the binding energy and bonding geometry of single H, F, and O atoms on the top Te site of α - and β -Te to obtain a deeper understanding of how adatom impurities interact with the Te surface. We also investigated the effects of single-molecule interaction of H₂, F₂, and O₂ with the bare α - and β -Te surfaces. For these calculations, we used a 4×4×1 supercell for α -Te and a 4×3×1 supercell for β -Te. We calculated the binding energy of the adatom (and H₂, F₂, and O₂ molecules) as $E_{binding} = (E_{Te+A,M} - E_{Te} - nE_{A,M})/n$, where $E_{Te+A,M}$ is the total energy of the Te sheet and the atom (A) or molecule (M) together, E_{Te} is the total energy of the bare Te sheet, $E_{A,M}$ is the total energy of the isolated atom or molecule, and n is the number of adatoms. The binding energies and charge transfer values are compiled in Table 1. We find that H, F, and O atoms bind

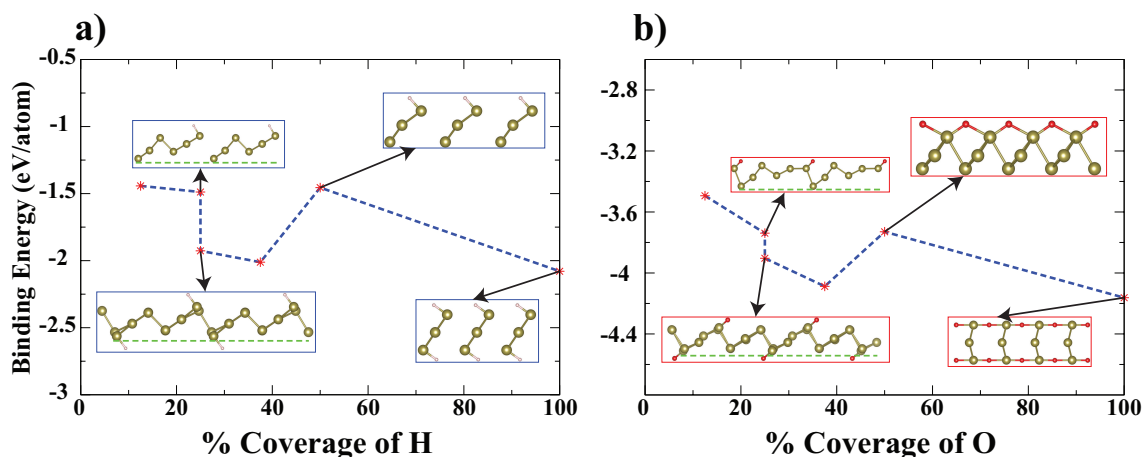


Fig. 4 Binding energy per adatom as a function of a) H and b) O coverage on β -Te. The figure insets depict the optimized structure for each coverage ratio.

Table 1 The binding or dissociation energies ($E_{binding/diss}$) of single H, O and F atoms and single H_2 , O_2 , and F_2 molecules on α and β -Te. The * indicates dissociation energy. Values of charge transferred to each adatom/molecule calculated from Bader charge analysis are also given.

Structure	$E_{binding/diss}$ (eV)	Bond Length (\AA)	Charge Transfer (e^-)
H on α -Te	-1.01	1.72	0.22
O on α -Te	-3.15	1.85	0.91
F on α -Te	-3.02	2.04	0.68
H on β -Te	-1.37	1.70	0.20
O on β -Te	-3.52	1.85	0.92
F on β -Te	-3.44	2.04	0.69
H_2 on α -Te	-0.02	3.38	0.00
O_2 on α -Te	-0.09	3.28	0.03
F_2 on α -Te	1.86*	-	0.66
H_2 on β -Te	-0.01	3.04	0.00
O_2 on β -Te	0.10	2.95	0.04
F_2 on β -Te	2.42*	-	0.64

directly above the Te atom top site of α -Te. However, for β -Te the H, F, and O atoms bond off center from the Te top site. For dilute concentration where adatom-adatom interactions are excluded, one can report that the dominant interaction is between the adatom and the nearest Te. Bond lengths, charge transfer values and binding energies show similar trend for both Te layered structures.

To obtain a clear picture of how adatom coverage impacts the stable Te structures (H- β -Te (local minimum) and O- β -Te), we varied the H and O coverage of a bare β -Te sheet (starting from the lattice parameters of β -Te). Coverage is calculated as: 12.5% for one adatom per a $2 \times 2 \times 1$ supercell, 25% for two adatoms per a $2 \times 2 \times 1$ supercell (we consider two atoms on one side, and one atom on each side), 37.5% for three adatoms per a $2 \times 2 \times 1$ supercell (one atom on one side and two atoms on the other side), 50% for 1 adatom per a $1 \times 1 \times 1$ cell, and 100% (full coverage) for 2 adatoms per a $1 \times 1 \times 1$ cell (one atom on each side). It is important to note that for certain coverage rates, there were multiple different adatom adsorption sites/combinations (different sites where O and H were placed) due to the symmetry of the β -Te sheet. We

considered three possible combinations for single sided 25%, four for double sided 25%, and two for 37.5%. For the coverage rates that had multiple adatom combinations, we reported just the lowest energy results. We relaxed each of these different configurations and calculated the binding energy per adatom (previously defined) as depicted in Figure 4. For both O and H functionalization, we observe the strongest binding energy for full coverage, indicating that full coverage is preferable on β -Te. As coverage increases, we see interesting trends in the binding energy and certain structural changes for H and O.

For varying H coverage, there is a disparity in the binding energy of single sided coverage versus double sided coverage. When we have H on only one side (25% (top data point) and 50% coverage in Figure 4), a distortion of the structure arises from the asymmetric placement of H atoms. For example at 25% single sided coverage, we see an upward bending of Te-Te bonds (the green dotted line is the x-axis for reference) that result in the bond breaking between periodic $2 \times 2 \times 1$ supercells. For 50% coverage, the one H atom on top of the $1 \times 1 \times 1$ β -Te cell results in a bending of the Te-Te bonds around the central Te atom. In comparison, the structures with H on both sides do not have this Te-Te bond bending due to the placement of H which reduces coulomb repulsion. This bond bending and structural transformations result in weaker H binding when compared to double sided coverage. However this sheds light on how functionalization occurs when a bare-Te sheet is already on a substrate, prior to functionalization. Also it is useful to note that we observe the separation of H- β -Te into uniform chains after 50% H coverage. For O coverage, we observe a similar trend in the binding energy. We again see an upward bending and distortion of the structure at 25% (single side) due to the asymmetry of the O distribution while the structure at 25% (double sided) has minimal distortion due to the presence of O on both sides. Significant structural reconstruction occurs between 50% and 100% coverage, including the breaking of the central Te bond, oxygen being fully embedded on both sides, and the buckling of the central Te atom. Again the disparity in the binding energies can be attributed to these structural transformations, with fully oxygenated (embedded) β -Te having

the strongest binding energy.

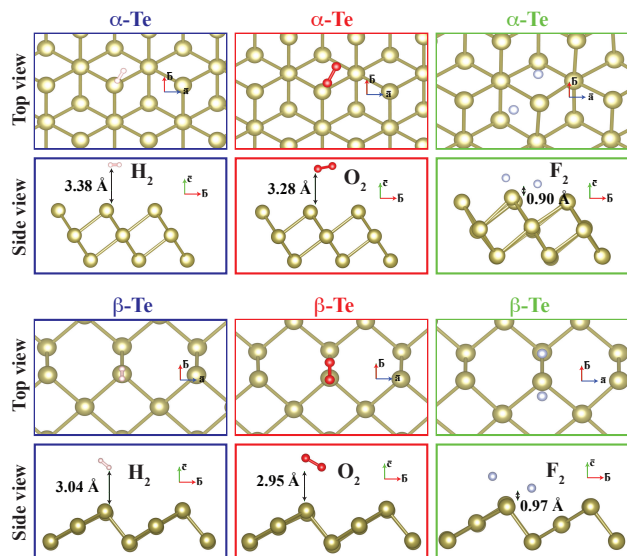


Fig. 5 The optimized geometry of 2D α and β -Te when single H_2 , O_2 and F_2 molecules are initially placed 2 Å above the surface.

To simulate single-molecule binding, we placed the molecule 2 Å above the bare Te surfaces and relaxed the structure (Figure 5). Single H_2 and O_2 molecules placed on one side of the α - and β -Te surfaces do not disrupt the Te structures and are physisorbed on the surface. There is not significant charge transfer due to this physisorption. In contrast, F_2 molecules dissociate on both the α - and β -Te surfaces. From this, we can infer that Te monolayers react strongly with fluorine. This conclusion is further supported by simulations of exposure of one or both sides of the Te structures to many F_2 molecules. MD simulations for these cases result in the destruction of the Tellurene layer (Figure S7). Because F_2 molecules dissociate on the Te surface, we instead calculated the dissociation energy for F_2 as $E_{\text{diss}} = E_{\text{binding},\text{F}_2} - 2E_{\text{binding},\text{F}}$ where $E_{\text{binding},\text{F}_2}$ is the binding energy of a single fluorine molecule and $E_{\text{binding},\text{F}}$ is the binding energy of a fluorine atom. The positive-valued dissociation energy is 1.86 eV for α -Te and 2.42 for β -Te, indicating that the dissociation of F_2 on either Tellurene surface is exothermic.

We extended our studies of Tellurene interaction with molecular hydrogen, oxygen, and fluorine by considering high coverage of H_2 , F_2 , and O_2 molecules placed on one or both sides of the α - and β -Te surfaces. We placed 8 molecules per side of a $4 \times 4 \times 1$ supercell of α -Te and 6 molecules per side of a $4 \times 3 \times 1$ supercell of β -Te, which results in coverage of $\sim 2 \times 10^{14} \text{ cm}^{-2}$ per side. Initially, molecules were randomly placed 2 Å above the bare Te surface. We performed MD simulations of these systems at 300 K with a timestep of 0.5 fs for 2 ps. Snapshots of the MD simulations are given in Fig. S7. As mentioned previously, F_2 molecules disrupt both α and β -Te monolayers. We see that H_2 molecules interact weakly with either Tellurene surface, with only a few molecules interacting via physisorption. For α -Te and β -Te, high concentrations of O_2 cause minor structural deformation of the Tellurene layer. From these results, we can confirm that α and β -Te remain

intact against H_2 and O_2 molecules while they are disrupted by F_2 .

3.4 Substrate effects

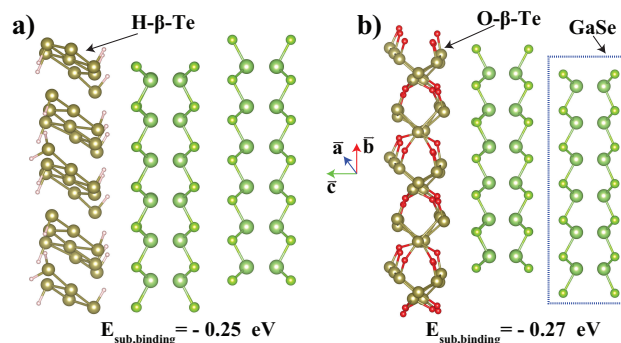


Fig. 6 The optimized geometry of a) $\text{H-}\beta$ -Te and b) $\text{O-}\beta$ -Te on top of a bilayer GaSe substrate.

As previously mentioned, Yang et al.⁴⁵ showed that Te sheets can be synthesized on a GaSe substrate, and from first principles that Te sheets bind strongly to the GaSe substrate. This motivated us to study the effects of substrates (in this case GaSe substrate) on our $\text{H-}\beta$ -Te (local minimum) and $\text{O-}\beta$ -Te (full and half-coverage) structures. The reason why we also include half coverage structures rely on the possibility that annealing or functionalization with O/H can take place when Te monolayers are on the substrate prior to chemical functionalization (where only one side is reactive).

In order to simulate these, we placed our functionalized β -Te (O or H) structures approximately 3 Å above bilayer GaSe, allowing the functionalized β -Te and the top layer of GaSe to relax, while keeping the bottom layer of GaSe static to mimic the continuous bulk GaSe substrate. The initial orientation of the Te monolayer on GaSe is chosen to have minimal lattice mismatch in a reasonable simulation size (less than ~ 600 atoms/ ~ 3000 electrons). This required a $2 \times 3 \times 1$ supercell of functionalized β -Te on top of a $3 \times 3 \times 1$ supercell of bilayer GaSe to minimize the lattice mismatch. For $\text{O-}\beta$ -Te on top of GaSe, the lattice mismatch ratio was 0.002 in the \vec{a} direction and 0.045 in the \vec{b} direction while for $\text{H-}\beta$ -Te, the lattice mismatch ratio was 0.046 in the \vec{a} direction and 0.079 in the \vec{b} direction. For sake of comparison, we also placed bare β -Te on top of GaSe, which required a $4 \times 7 \times 1$ supercell of β -Te and a $7 \times 8 \times 1$ supercell of bilayer GaSe to minimize lattice mismatch ratio. For the bare β -Te on top of GaSe, the mismatch ratio was 0.032 in the \vec{a} direction and 0.044 in the \vec{b} direction. It is important to note that the shape and orientation (about the \vec{a} axis) of the Te monolayers are free to relax during geometry optimization.

Figure 6 depicts the relaxed structure of a) $\text{H-}\beta$ -Te (local minimum) and b) $\text{O-}\beta$ -Te on top of bilayer GaSe. For the $\text{H-}\beta$ -Te case, we observe that the $\text{H-}\beta$ -Te separated chains are fully intact and oriented along slightly tilted \vec{a} direction on top of GaSe. We also see that when $\text{O-}\beta$ -Te is placed on top of GaSe, it retains its Te_3O_2 -like structure with oxygen embedding itself inside the

Te layers and a buckling of the central Te atom. The Te_3O_2 -like structure prefers to align (no twisting in the \vec{a} direction) with the underlying GaSe layer. Additionally, the top layer of GaSe is not disrupted by either functionalized Te structure. Likewise, when bare β -Te is placed on bilayer GaSe, it is not disrupted but largely twisted from GaSe along the \vec{a} direction upon structural optimization as indicated in Fig. S8g).

We define the substrate binding energy as $E_{\text{sub, binding}} = E_{M, \text{Te} + \text{GaSe}} - E_{M, \text{Te}} - E_{\text{GaSe}}$, where $E_{M, \text{Te} + \text{GaSe}}$ is the energy of the functionalized Te on top of bilayer GaSe, $E_{M, \text{Te}}$ is the energy of the isolated functionalized (or bare) Te layer, E_{GaSe} is the energy of the isolated bilayer GaSe and M represents either O or H atoms (or bare). From this, we obtain a substrate binding energy (per formula unit) of -0.25 eV for H- β -Te and -0.27 eV for O- β -Te, indicating that the binding mechanism between functionalized Te structures to the GaSe substrate is similar to physisorption. We also considered H- β -Te and O- β -Te with 50% coverage (one case with the adatoms on the side of Te facing the GaSe substrate, and the other case where the adatoms are on the opposite side of Te) which are depicted in Figure S8. For the case where the adatoms are on the side of Te facing GaSe, the binding energies of H- β -Te and O- β -Te are -0.25 eV and -0.34 eV respectively. For the case with the adatoms on the side opposite to Te, the binding energies of H- β -Te and O- β -Te are -0.27 eV and -0.27 eV, proving that 50% coverage of adatoms on either side has a comparable substrate binding energy to full coverage. We also calculated the substrate binding energy of bare β -Te on bilayer GaSe to be -0.35 eV (per formula unit).

To confirm our claim of GaSe being a suitable substrate for these Te structures, we calculated the charge difference isosurfaces between functionalized Te (H- β -Te and O- β -Te for full and half coverage) and GaSe in addition to the charge difference between bare β -Te and GaSe, depicted in Fig. S8. For all structures, we see an accumulation of charge primarily between the Te layer and the side of GaSe facing the Te layer from p_z orbitals of the corresponding Te and Se atoms. This transfer of electrons confirms that there is a charge sharing between Te and substrate, and that even less favorable half-functionalized Te structures can still bind on and become stabilized on bilayer GaSe. The bonding mechanism between bare Te monolayer and half functionalized β -Te (adatoms opposite site of Te) are similar. In the case of half functionalized β -Te where adatoms are facing the substrate, we observed that H atoms are creating bonds between Se's of the substrate and β -Te. Since O adatoms prefer to embed inside Te monolayers, the bonding with the substrate is still between p_z orbitals of the corresponding Te and Se atoms. However, charge accumulation at the boundary of functionalized Te and the substrate is not resulting in a net charge transfer between the substrate and functionalized Te layers according to the Bader charge analysis^{32,33}. Even though we try to use the largest supercells computationally possible with our resources, the slight variation on binding energies should be expected if simulations are done with different supercell sizes. From these results, we can confidently propose GaSe as a viable substrate for bare β -Te and its O and H functionalized counterparts.

To demonstrate that the electronic properties of functionalized

Te are unaffected by the GaSe substrate and the binding is dominantly physisorption, we calculated the DOS of free-standing O- β -Te and H- β -Te and calculated the DOS of O- β -Te and H- β -Te on top of the GaSe (just taking the projected monolayer DOS), depicted in Fig. S9. From this figure we see that the DOS of the free-standing monolayer and the DOS of the monolayer on the substrate are practically unchanged. Since we have low binding energy per formula unit and similar electronic properties in both free-standing and on substrate cases, including no net charge transfer between the substrate and the functionalized Te layer, we conclude that the binding mechanism between functionalized Te and GaSe substrate is dominantly physisorption. We know from experiments, that 2D Te structures must be synthesized on a substrate and don't exist in free-standing form. Since our findings indicate that the substrate has minimal effect on the electronic properties of these Te structures, our predictive results of free-standing Te outlined in the previous sections can be useful for experimentalists who are interested in synthesizing these materials.

3.5 Conclusion

We have provided a comprehensive study of the electronic properties of 2D Tellurene structures including bare and functionalized (with H, O, and F) α - and β -Te monolayers. We find that functionalization results in significant structural changes for monolayer Te such as disruption of the structure of α -Te by H, O, and F; separation of β -Te into functionalized chains by H and F; and the complete transformation of β -Te into a metallic Te_3O_2 -like structure by O. The functionalization of these α and β -Te monolayers also result in metallic properties for all structures except H- β -Te, which has a band gap of 1.37 eV and can be utilized for devices in the near infrared range. Coverage results indicate that fully functionalized H- β -Te and O- β -Te have the strongest adatom binding energies. We also studied the effect of H- β -Te and O- β -Te on a GaSe substrate and found that these structures bind strongly and remain undisrupted when on top of bilayer GaSe, indicating that GaSe is a promising candidate as a substrate material for functionalized 2D monolayers and enhances the stability of functionalized Te monolayers. Our results, in addition to the recent experimental progress in synthesizing Te structures, prove that bare and functionalized 2D Te structures are viable candidates for next generation optoelectronic devices and can be used as metallic contacts in nanoscale junctions.

4 Acknowledgments

Part of the calculations have been carried out at UMBC High Performance Computing Facility (HPCF). This work was supported by the National Science Foundation through Division of Materials Research under NSF DMR-1726213 Grant.

Notes and references

- 1 G. Fiori, F. Bonaccorso, G. Iannaccone, T. Palacios, D. Neumaier, A. Seabaugh, S. K. Banerjee and L. Colombo, *Nature Nanotechnology*, 2014, **9**, 768.
- 2 J. Kang, W. Liu, D. Sarkar, D. Jena and K. Banerjee, *Phys. Rev.*

- X, 2014, **4**, 031005.
- 3 F. Schwierz, J. Pezoldt and R. Granzner, *Nanoscale*, 2015, **7**, 8261–8283.
- 4 S. Zhang, Z. Yan, Y. Li, Z. Chen and H. Zeng, *Angewandte Chemie International Edition*, **54**, 3112–3115.
- 5 F. Ersan, E. Aktürk and S. Ciraci, *Phys. Rev. B*, 2016, **94**, 245417.
- 6 S. Cahangirov, M. Topsakal, E. Aktürk, H. Şahin and S. Ciraci, *Phys. Rev. Lett.*, 2009, **102**, 236804.
- 7 Z. Zhu, X. Cai, S. Yi, J. Chen, Y. Dai, C. Niu, Z. Guo, M. Xie, F. Liu, J.-H. Cho, Y. Jia and Z. Zhang, *Phys. Rev. Lett.*, 2017, **119**, 106101.
- 8 X. Huang, J. Guan, Z. Lin, B. Liu, S. Xing, W. Wang and J. Guo, *Nano Letters*, 2017, **17**, 4619–4623.
- 9 Y. Du, G. Qiu, Y. Wang, M. Si, X. Xu, W. Wu and P. D. Ye, *Nano Letters*, 2017, **17**, 3965–3973.
- 10 Y. Wang, G. Qiu, R. Wang, S. Huang, Q. Wang, Y. Liu, Y. Du, W. A. Goddard, M. J. Kim, X. Xu, P. D. Ye and W. Wu, *Nature Electronics*, 2018, **1**, 228–236.
- 11 L. Xian, A. P. Paz, E. Bianco, P. M. Ajayan and A. Rubio, *2D Materials*, 2017, **4**, 041003.
- 12 S. Khatun, A. Banerjee and A. J. Pal, *Nanoscale*, 2019, **11**, 3591–3598.
- 13 S. Sharma, N. Singh and U. Schwingenschlögl, *ACS Applied Energy Materials*, 2018, **1**, 1950–1954.
- 14 G. Qiu, Y. Wang, Y. Nie, Y. Zheng, K. Cho, W. Wu and P. D. Ye, *Nano Letters*, 2018, **18**, 5760–5767.
- 15 M. Amani, C. Tan, G. Zhang, C. Zhao, J. Bullock, X. Song, H. Kim, V. R. Shrestha, Y. Gao, K. B. Crozier, M. Scott and A. Javey, *ACS Nano*, 2018, **12**, 7253–7263.
- 16 Y. Dong, B. Zeng, X. Zhang, D. Li, J. He and M. Long, *Journal of Applied Physics*, 2019, **125**, 064304.
- 17 Y. Xiang, S. Gao, R.-G. Xu, W. Wu and Y. Leng, *Nano Energy*, 2019, **58**, 202 – 210.
- 18 X. H. Wang, D. W. Wang, A. J. Yang, N. Koratkar, J. F. Chu, P. L. Lv and M. Z. Rong, *Phys. Chem. Chem. Phys.*, 2018, **20**, 4058–4066.
- 19 S. Zhang, W. Zhou, Y. Ma, J. Ji, B. Cai, S. A. Yang, Z. Zhu, Z. Chen and H. Zeng, *Nano Letters*, 2017, **17**, 3434–3440.
- 20 Z. Song, C.-C. Liu, J. Yang, J. Han, M. Ye, B. Fu, Y. Yang, Q. Niu, J. Lu and Y. Yao, *Npg Asia Materials*, 2014, **6**, e147.
- 21 Y. Li and X. Chen, *2D Materials*, 2014, **1**, 031002.
- 22 Y.-p. Wang, W.-x. Ji, C.-w. Zhang, P. Li, F. Li, M.-j. Ren, X.-L. Chen, M. Yuan and P.-j. Wang, *Scientific Reports*, 2016, **6**, 20342.
- 23 D. W. Boukhvalov, A. N. Rudenko, D. A. Prishchenko, V. G. Mazurenko and M. I. Katsnelson, *Phys. Chem. Chem. Phys.*, 2015, **17**, 15209–15217.
- 24 M.-Y. Liu, Z.-Y. Li, Q.-Y. Chen, Y. Huang, C. Cao and Y. He, *Scientific Reports*, 2017, **7**, 4773.
- 25 S. Zhou, C.-C. Liu, J. Zhao and Y. Yao, *npj Quantum Materials*, 2018, **3**, 16.
- 26 G. Kresse and J. Furthmüller, *Phys. Rev. B*, 1996, **54**, 11169–11186.
- 27 P. E. Blöchl, *Phys. Rev. B*, 1994, **50**, 17953–17979.
- 28 S. Grimme, *Journal of Computational Chemistry*, 2006, **27**, 1787–1799.
- 29 J. P. Perdew, K. Burke and M. Ernzerhof, *Phys. Rev. Lett.*, 1996, **77**, 3865–3868.
- 30 H. J. Monkhorst and J. D. Pack, *Phys. Rev. B*, 1976, **13**, 5188–5192.
- 31 A. Togo and I. Tanaka, *Scripta Materialia*, 2015, **108**, 1 – 5.
- 32 R. F. W. Bader, in *Atoms in Molecules*, American Cancer Society, 2002.
- 33 G. Henkelman, A. Arnaldsson and H. Jónsson, *Computational Materials Science*, 2006, **36**, 354–360.
- 34 K. Momma and F. Izumi, *Journal of Applied Crystallography*, 2011, **44**, 1272–1276.
- 35 G. K. Madsen, J. Carrete and M. J. Verstraete, *Computer Physics Communications*, 2018, **231**, 140 – 145.
- 36 G. K. Madsen and D. J. Singh, *Computer Physics Communications*, 2006, **175**, 67 – 71.
- 37 M. Mantina, A. C. Chamberlin, R. Valero, C. J. Cramer and D. G. Truhlar, *The Journal of Physical Chemistry A*, 2009, **113**, 5806–5812.
- 38 C.-H. Cheung, H.-R. Fuh, M.-C. Hsu, Y.-C. Lin and C.-R. Chang, *Nanoscale Research Letters*, 2016, **11**, 459.
- 39 Y. Chen, J. Liu, J. Yu, Y. Guo and Q. Sun, *Phys. Chem. Chem. Phys.*, 2019, **21**, 1207–1216.
- 40 D. K. Sang, B. Wen, S. Gao, Y. Zeng, F. Meng, Z. Guo and H. Zhang, *Nanomaterials (Basel, Switzerland)*, 2019, **9**, 1075.
- 41 C. Lin, W. Cheng, G. Chai and H. Zhang, *Phys. Chem. Chem. Phys.*, 2018, **20**, 24250–24256.
- 42 S. Yi, Z. Zhu, X. Cai, Y. Jia and J.-H. Cho, *Inorganic Chemistry*, 2018, **57**, 5083–5088.
- 43 O. I. Malyi, K. V. Sopiha and C. Persson, *ACS Applied Materials & Interfaces*, 2019, **11**, 24876–24884.
- 44 J. Yan, X. Zhang, Y. Pan, J. Li, B. Shi, S. Liu, J. Yang, Z. Song, H. Zhang, M. Ye, R. Quhe, Y. Wang, J. Yang, F. Pan and J. Lu, *J. Mater. Chem. C*, 2018, **6**, 6153–6163.
- 45 S. Yang, B. Chen, Y. Qin, Y. Zhou, L. Liu, M. Durso, H. Zhuang, Y. Shen and S. Tongay, *Phys. Rev. Materials*, 2018, **2**, 104002.
- 46 T. Paulauskas, F. G. Sen, C. Sun, Y. Zhang, S. Hla, P. Longo, M. J. Kim, M. Chan and R. F. Klie, *Nanoscale*, 2019, 14698–14706.